ADVANCED ENGINEERING MATERIALS

COMMUNICATION

DOI: 10.1002/adem.201200075

On the Correlation Between Thermal Cycle and Formation of Intermetallic Phases at the Interface of Laser-Welded Aluminum-Steel Overlap Joints**

By *Agnieszka Szczepaniak, Jianfeng Fan, Aleksander Kostka** and *Dierk Raabe*

A laser beam welding process via heat conduction was applied to join DC01 steel with aluminum (Al) in overlap configuration without filler wire. The effect of the applied laser power (1.7, 1.8, 2.1, and 2.4 kW) on the formation and evolution of the interfaces between steel and Al was analyzed. Two intermetallic compounds were found at the interface, namely, one adjacent to the steel layer (Al_5Fe_2) and one close to the solidified Al ($Al_{13}Fe_4$). The thickness of the intermetallic reaction layer increases with laser power, while the morphology of its individual components evolves due to differences in accumulated thermal cycles. Correlations between simulations and measurements show that the peak temperature has significantly stronger influence on the thickness of the intermetallic reaction layer than cooling time and the integral of temperature over the time. Shear/tensile strength tests reveal that all the specimens fail in the Al heat affected zone.

Iron (Fe) and aluminum (Al) alloys can provide an excellent combination of good properties (low density and/or good corrosion resistance for Al alloys and good formability and strength for steel) at low material costs, therefore, dissimilar joints between them are of significant importance in engineering applications. Producing reliable and cost effective dissimilar joints between these important engineering materials, hence, requires better metallurgical understanding of the joining techniques and their specific influence on the resulting microstructures. One of the main pending challenges, both from a scientific and an applied point of view is the formation of brittle Al_xFe_y intermetallics during joining of steels to Al alloys. The formation and growth of the intermetallic phases (IMPs) between the liquid Al and the solid steel is governed both by chemical reaction and by interdiffusion.[1–4] IMPs which form on the joined interface have been found to be detrimental to the properties of joints between Al and Fe/steel and, hence, it is of general interest to limit their thickness.[4–8]

According to the Al–Fe phase diagram,[9] IMPs can form in a wide range of element concentrations and temperatures. However, as described by Kidson,[10] the phase formation depends on three subsequent factors: (1) the chemical potentials, (2) the nucleation conditions at the beginning of the interdiffusion, and (3) the mobility of the constituent elements. The latter two factors imply that not all phases present in the phase diagram will necessarily appear as reaction products of the thermal joining.

The dominant reaction product at the interface between Fe and Al is the orthorhombic Al_5Fe_2-phase which growth following a parabolic law in the temperature range of 990–1215 K.[11] Second, a frequently observed component of the interfacial reaction layer is the monoclinic $Al_{13}Fe_4$-phase (also referred to as Al_3Fe) which typically occurs between Al and Al_5Fe_2.[1,2] Rapid cooling associated with the laser joining can influence the formation and growth of reaction layers at the interface region. Rapidly solidified Fe–Al alloys may exhibit metastable intermetallic compounds such as Al_9Fe_2 and Al_6Fe.

Among a wide range of thermal methods, laser welding is an established joining technique due to its advantages such as low distortion, high welding speed, and good seam quality.[5,12–14] Especially in joining of dissimilar metals, its high power density but low heat input process is much more beneficial.[15] During the last years different welding processes for hybrid joints have been developed.[16] A laser welding process via heat conduction was successfully applied in Al–steel hybrid joints.[17]

[*] *A. Szczepaniak, Dr. A. Kostka, Prof. D. Raabe*
Max-Planck-Institut für Eisenforschung GmbH, 40237 Düsseldorf, Germany
E-mail: a.kostka@mpie.de
J. Fan
BIAS-Bremer Institut für angewandte Strahltechnik GmbH, 28359 Bremen, Germany

[**] *The work presented in this paper is part of the project ''Investigation and characterization of the IMP formation of dissimilar Fe–Al joints produced by fast laser-based joining process with large temperature gradients'' (KO 3998/1-1). The authors gratefully thank the DFG for supporting this project.*

ADVANCED ENGINEERING MATERIALS

Only one of the joint components is melted here, and the high process velocity, which reduces the heat input in the contact zone, leads to a small thickness of the intermetallic reaction layer of several μm. The heat input (laser power divided by welding speed) is commonly used in the welder society to describe the correlation between the mechanical properties and the microstructure of the interface (the amount and morphology of IMPs). Yet, the resulting microstructure is also highly affected by the overall heat flow in the contact zone (which depends on the applied process configuration). The heat flow depends on the applied process configuration and influences heating and cooling rates, and hence, the diffusion time. Thus to analyze the growth mechanisms of the intermetallic layer – the thermal cycle (defined by peak temperature, cooling time, and integral of temperature over time) needs to be taken to consideration.

The technical details associated with the exact measurement of the thermal energy dissipation in the welded configuration justified the development of numerical modeling methods of the heat flow. Based on the known parameters (thermo-physical properties, energy input, and heat loss) it is possible to simulate the thermal cycle in the non-accessible contact zone between two base materials, where the IMP layer is formed.

Characterization and understanding of the growth mechanisms of Fe_xAl_y-phases are essential to improve the joining parameters and ultimately replace mechanical bonding by chemical bonding of Al-to-steel hybrid parts. The scope of this work is to show the correlation between the thermal cycle and the formation of IMPs during laser joining of Al-to-steel. Main attention is placed on identification and characterization of the rapid thermal cycles resulting from the applied configuration and welding parameters. Specific emphasis is placed on the influence of peak temperature, cooling time, and the integral of thermal cycle on formation and evolution of the intermetallic reaction layer.

1. Materials, Experiment, and Simulation Procedures

A DC01 low carbon steel and Al99.5 (of 99.5 wt% purity) Al alloy plates were joined using a laser beam in overlap configuration at the Bremer Institut für Angewandte Strahltechnik GmbH. Selected materials of simple chemical composition prevent formation of complex intermetallic compounds in the reaction layer. Chemical composition of both materials determined by wet chemical analysis is given in the Table 1.

A heat conduction welding using a 4 kW Nd:YAG laser Trumpf HL4006D was applied in this study. For the configuration shown in Figure 1 following welding parameters were chosen: 1.7, 1.8, 2.1 and 2.4 kW laser power; constant speed of 0.8 m · min^{-1}. (12 s per joint); 5.63 mm laser spot diameter; F 400 NH flux and Argon (40 L · min^{-1}) shielding gas atmosphere. The 0.75 mm thick steel sheet was placed above the 1 mm thick Al sheet, whereby a 4 mm wide overlap was prepared. Both sheets have a width of 100 mm and a length of 200 mm. The transverse direction (TD) of the steel plate and the rolling direction (RD) of the Al plate were parallel to the welding direction (Figure 1). During welding, the heat adsorbed by the steel sheet was transferred to the Al plate. Only the Al was molten, and the joint was created by the wetting of liquid Al to the solid steel.

Table 1. Chemical composition (in wt%) of the base materials used in this study.

Material	Fe	C	Mn
DC01	Bal.	0.037	0.175
Material	Al	Fe	Si
Al99.5	Bal.	0.37	0.065

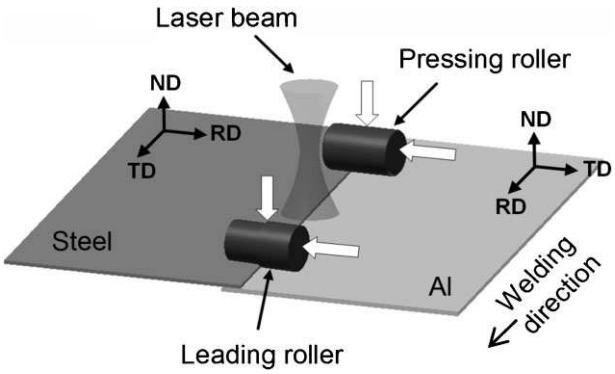

Fig. 1. Schematic illustration of the welding configuration and spatial arrangement of Al and steel plates: RD, rolling direction; TD, transverse direction; ND, normal direction.

Besides, a pressure unit consisting of two rollers was applied to ensure optimal contact between the joined components (Figure 1). The pressing rollers eliminated a possible air gap between the two sheets, so that the heat input absorbed by the steel sheet could be transferred directly to the Al. The leading roller was positioned at the edge of the steel sheet, and due to the lateral pressure, an automatic tracking of the joint was realized.

Two different techniques were applied during welding for simultaneous temperature measurements (Figure 2). A thermocouple type K was fixed under the Al sheet (through a hole of 1.1 mm diameter) measuring the temperature at point A. The signal of the thermocouple was converted to

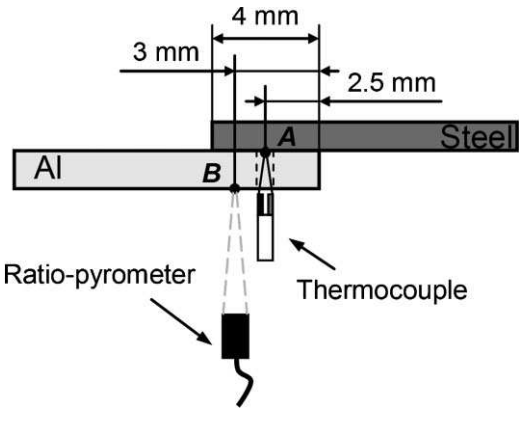

Fig. 2. Setup of temperature measurements at point A and B.

temperature by a data logger OMEGA DAQ 3000. At the same time, a ratio-pyrometer (Igar 12 LO) was located under both joined components, measuring the temperature at point B.

The heat transfer simulations were carried out using the Abaqus/Standard FEM software in conjunction with the following assumptions and boundary conditions: (1) isotropic material properties; (2) temperature-dependent heat capacity and thermal conductivity, but constant absorption coefficient; (3) mechanical constraints caused by the clamping and pressure unit were neglected; (4) the change of the geometry, that is, the weld seam during the welding was neglected; (5) heat loss by convection and radiation was modeled by Newton's law of cooling and the Stefan–Boltzmann law, respectively; (6) the element type is DC3D8 and the quasi-Newton solution technique was chosen [18]; (7) microstructural transformation was not taken into consideration.

The FE-simulations were calibrated and validated by the measured temperatures using the thermocouple and ratio-pyrometer described above.

Specimens for microstructure characterization and tensile testing were cut across the 150 mm-long weld (Figure 3) by spark erosion.

Metallographic microsections were prepared as cross-sections in the weld zones of samples marked as B in Figure 3. Specimens were grinded with SiC and then polished with 3 μm diamond paste. The final-polishing using SiO_2 suspension was applied to obtain a deformation-free surface required for the electron back scattered diffraction (EBSD) analysis. The microstructure investigations were carried out using a Jeol JSM-6500F field emission scanning electron microscope (SEM) operated at 15 kV equipped with TSL EBSD and an EDAX energy-dispersive X-ray spectroscopy (EDS) system.

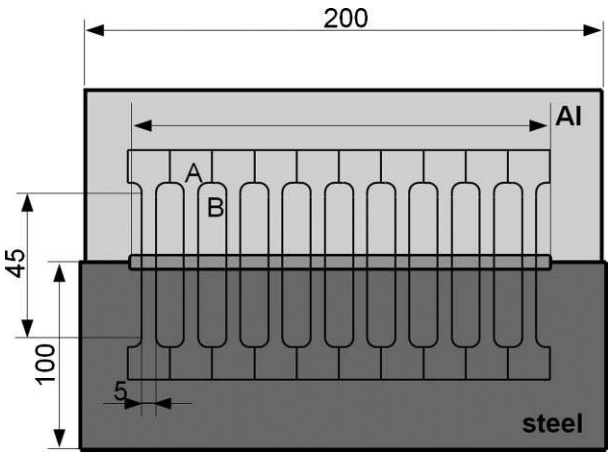

Fig. 3. Illustration of a welded joint sectioning for microstructural and mechanical testing: A, samples for tensile testing; B, samples for microstructure characterization.

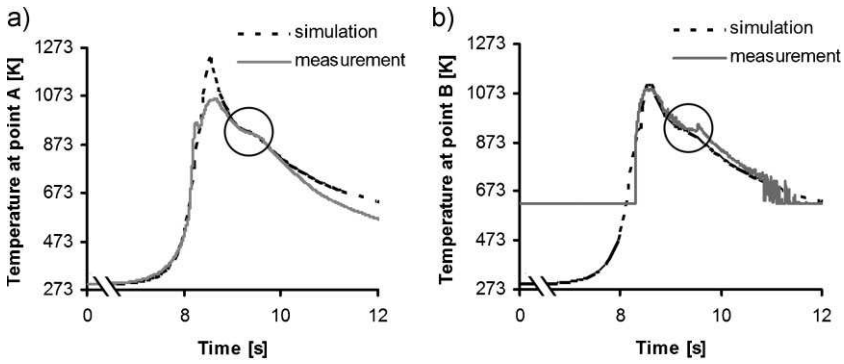

Fig. 4. Comparison of measured and FEM-simulated thermal cycles at measuring points A (a) and B (b). Circles indicate the melting point of Al (935 K).

2. Results

2.1. Heat Input Measurements and Simulations

Figure 4 presents measured and simulated thermal cycles of the joints produced with 2.1 kW laser power, 0.8 m · min^{-1} process velocity, and 5.63 mm spot diameter. We point out that the ratio-pyrometer can only measure temperatures above 625 K, and therefore only noisy data are available toward the end of the measurement (Figure 4b). The heating rate slope at point A can reach about 2200 K · s^{-1}, compared to 1800 K · s^{-1} at point B. The maximum temperature measured by the thermocouple at the interface region (at point A in Figure 2) is about 973 K, which is lower than the temperature measured by the ratio-pyrometer at the bottom side of the Al plate (at point B in Figure 2). Moreover, both measured cooling curves reveal a change in the cooling rate around the melting point of Al (935 K – marked by circles in Figure 4). This is due to the latent heat released during the phase change, that is, from liquid to solid Al.

Since precise values of the thermal cycle (the peak temperature, cooling time, and integral of the temperature over time) at the interface region (e.g., point A in Figure 2) are critical boundary condition parameters for the investigation of the thickness of the IMP layer, corresponding heat transfer simulations were performed. The simulated and measured thermal cycles at points A and B are also presented in Figure 4. We observe a good agreement between curves presenting simulated and the measured temperature during cooling around 935 K in Figure 4a, because the latent heat was taken into account in the simulation. However, the simulated temperature peak at point A differs significantly from the measurement. In Figure 4b, the simulated thermal cycle at point B shows a good match to the measurement.

From the simulated thermal cycle at point A, the peak temperature, cooling time, and integral of the temperature over time can be derived. We emphasize that only the thermal cycle above 625 K is taken into account, because the formation of IMPs takes place mainly in the temperature range above 625 K.[19] Figure 5 shows the influence of the laser power on these three properties. It is clear that peak temperature,

ADVANCED ENGINEERING MATERIALS

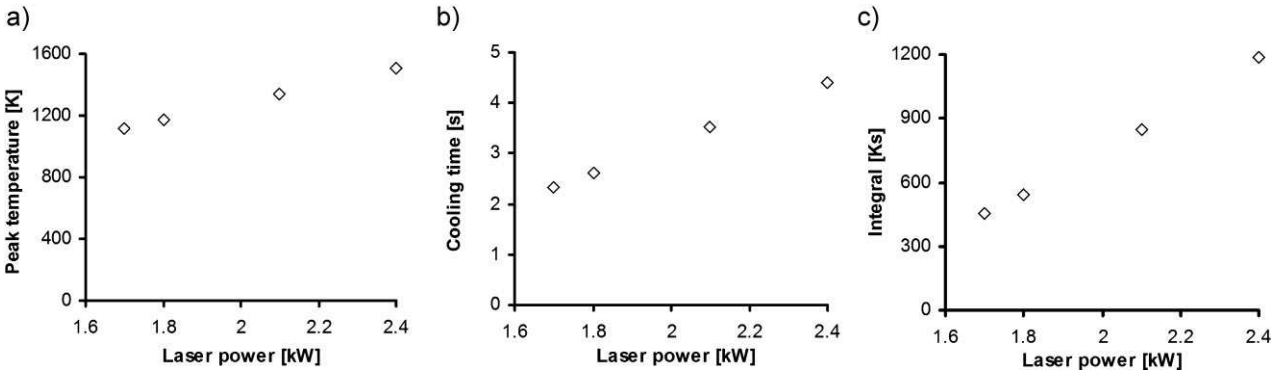

Fig. 5. Influence of the laser power on peak temperature (a), cooling time (b), and the time integral of thermal cycle (c) at point A based on the FEM simulation results.

cooling time, and their respective integral of the imposed thermal cycle are increasing linearly with the laser power.

2.2. Weld Microstructures and Properties

Welding does not only provide the metallic bonding at the interface,[20] but also modifies the microstructure of both parent materials within the heat affected zone (HAZ). The macroscopic examination of cross-sections reveals a good microstructural quality of the welds and the affected zones around it without any macroscopic defects. Figure 6 shows an EBSD inverse pole figure map of a cross-sectional area of the joint. The colors represent the particular crystallographic directions parallel to a reference direction of the grains. Four zones of distinctly different microstructures can be distinguished in the Al plate (Figure 6): (1) equiaxed grains, (2) and (4) elongated grains, and (3) large equiaxed grains. Grains present in zone 2 are characterized by gradients in shape and elongation. In contrast, grains in zone 4 are only slightly elongated. The microstructure of the steel plate shown in Figure 6 is divided into three sections: zone A is mainly composed of grains of a diameter between 3 and 9 μm, fine grains of an average diameter of 5 μm are observed in zone B. The presence of the huge gradient in the grains size is characteristic for zone C. The biggest grains in this area can reach 100 μm in diameter.

In order to characterize the components of the reaction layer formed in the interface region of the joints a high resolution EBSD analysis was conducted. Figure 7 displays an exemplary part of the EBSD microstructure analysis composed of the phase map (Figure 7a) and the crystallographic orientation map (Figure 7b). According to the phase map, a thin layer of the reaction products is formed at the interface between the steel base material (on the top of Figure 7a) and the Al (bottom of the same figure). Figure 7a reveals that the interlayer consists of two intermetallic compounds, namely, the orthorhombic Al_5Fe_2-phase adjacent to the steel and monoclinic $Al_{13}Fe_4$-phase adjacent to the Al. The layer of Al_5Fe_2-phase is significantly thicker than the $Al_{13}Fe_4$ layer. The Al_5Fe_2-phase presented in Figure 7 is composed of columnar grains. Crystals of the $Al_{13}Fe_4$-phase are smaller and also elongated. The $Al_{13}Fe_4$-phase can also occur in the form of the plate-like precipitations redistributed in the Al matrix near the interface. Plates of the $Al_{13}Fe_4$-phase that are not connected to the interlayer were not counted as part of the layer in the measurement of the layer thickness. Regarding Figure 7b all crystals of the Al_5Fe_2-phase are oriented parallel

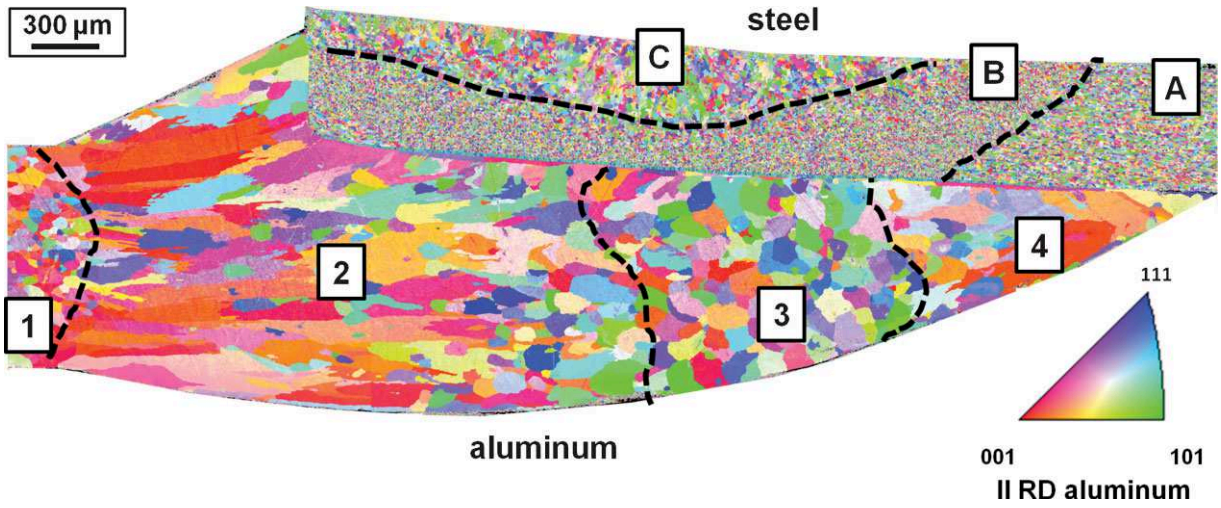

Fig. 6. Montage of EBSD crystallographic orientation maps showing the cross-section of the entire joint divided into seven distinct microstructural zones representing variations in morphology of Al and steel microstructure. The joint was produced with a laser power of 2.1 kW. The unit triangle shows the crystallographic poles aligned with the Al plate RD.

COMMUNICATION

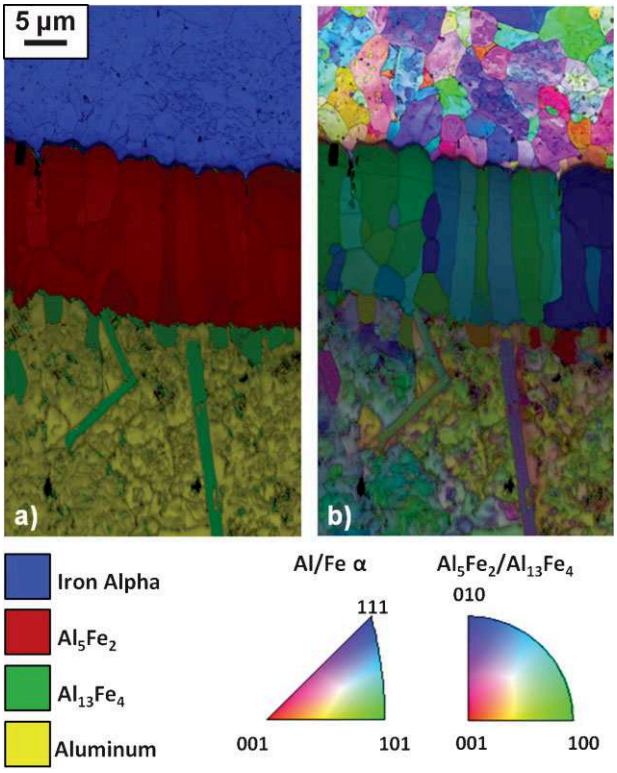

Fig. 7. EBSD analysis of the reaction layer of the joint welded with a laser beam of 2.4 kW power: (a) phase map and (b) inverse pole figure orientation map. Both maps are superimposed with the gray scale image quality map (the image quality describes the quality of a collected diffraction pattern indicating lattice defect density); the image quality map compiles the image quality obtained for each point in the analyzed area; darker gray shades indicate lower and brighter shades point out higher quality of the pattern.

to the crystallographic [001] direction. Grains of $Al_{13}Fe_4$ are randomly oriented.

Figure 8 compiles representative examples of the interface reaction layers formed at different laser power values. It can be perceived that the amount of reaction products increases with the rise of the laser power. Increase in the amount of applied heat changes both: the thickness and the morphology of the layer.

The corresponding values of the average intermetallic layer thickness (both intermetallic compounds) determined from the SEM micrographs are presented in Figure 9. Thickness

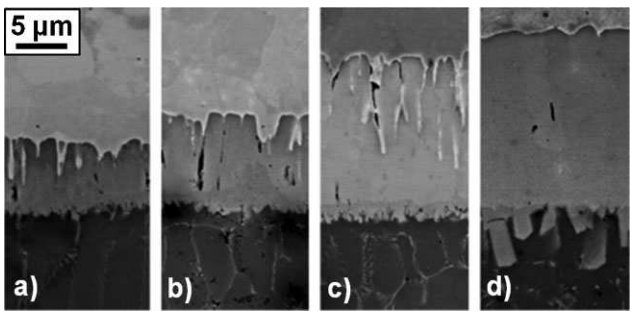

Fig. 8. SEM secondary electron (SE) micrographs of cross-sections of steel–Al joints obtained by welding with laser power values: (a) 1.7 kW, (b) 1.8 kW, (c) 2.1 kW, and (d) 2.4 kW.

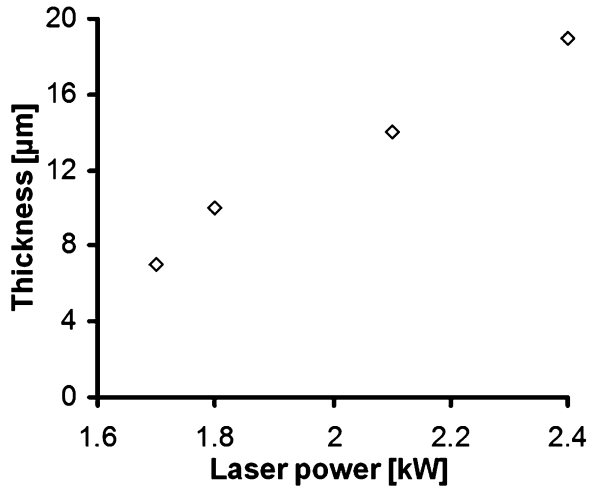

Fig. 9. The layer thickness of the formed intermetallic compounds as a function of a laser power.

measurements show that 40% increase of laser power (from 1.7 to 2.4 kW) results in increase of interlayer thickness of about 170%. The layer thickness does not grow linearly with the applied laser power though. The increase in the laser power from 1.7 to 1.8 kW (of 6%) causes an overall layer thickness increase of 43%. However, 14% increase of the laser power (from 2.1 to 2.4 kW) causes only 36% growth in the layer thickness.

The representative measurement of thickness of both intermetallic compounds shown in Figure 8 is challenging due to the weak contrast between the abutting phases that was obtained in the SEM micrographs. However, in all studied joints we observed that the thickness of the Al_5Fe_2-phase was significantly larger than that of the $Al_{13}Fe_4$-phase.

The well-known wavy morphology[1–3,21,22] of the interface between the steel and the intermetallic layer is due to the finger-like shape of the Al_5Fe_2 grains, oriented toward the steel plate. Figure 10 presents the SEM micrographs of samples welded with a laser beam power 1.7 kW (Figure 10a) and 2.4 kW (Figure 10c). In both samples the interface between the steel and the Al_5Fe_2 layer is irregular. Particularly, the observed irregularities are more pronounced in the sample presented in Figure 10a. Comparing the morphology of the steel/Al_5Fe_2 interfaces presented in Figure 10a and c it can be concluded that the interface tends to flatten when the laser power increases.

Moreover the morphology of the $Al_{13}Fe_4$-phase is affected by the applied laser power: As can be seen in Figure 10a crystallites of $Al_{13}Fe_4$ create a continuous layer that separates the Al_5Fe_2-phase from the Al. Fine, equiaxed particles of the $Al_{13}Fe_4$ appear along the interface with the Al (Figure 10b). A serrated morphology of $Al_{13}Fe_4$/Al boundary presented in Figure 10c reflects the shape of the $Al_{13}Fe_4$ grains attached to the Al_5Fe_2 layer. As can be observed in Figure 10c the $Al_{13}Fe_4$-phase consists of small plates crystals.

Besides the mere characterization of the microstructural changes associated with welding we aim at establishing more

ADVANCED ENGINEERING MATERIALS

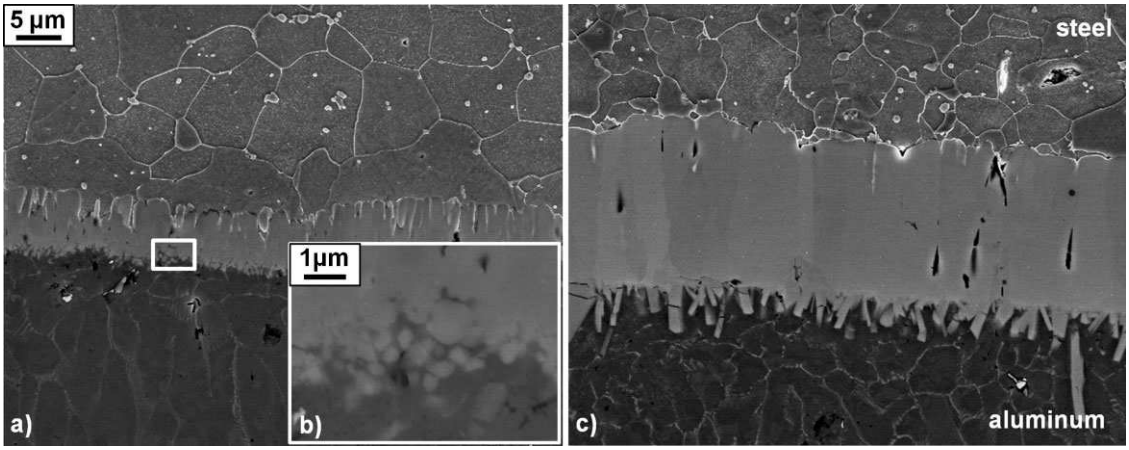

Fig. 10. SEM micrographs showing the interfaces $Al/Al_{13}Fe_4$ and steel/Al_5Fe_2 in samples welded with a laser power of: (a) 1.7 kW and (c) 2.4 kW. (b) Higher magnification view of the area marked by the white rectangle in (a). Etched with 1% Nital.

systematic microstructure-properties relationships between joining processes and mechanical behavior. Therefore, we conducted additional systematic mechanical tests to evaluate properties of joints. Mechanical tests were carried out using the Instron 85511 machine to subject the selected specimens to a tensile–shear test. Plates of a thickness 0.8 and 1 mm were additionally placed in the clamps on the side of the Al and the steel part of the welded sample, respectively, to compensate the off-center moment. These tensile–shear tests performed at room temperature in initial strain rate $10^{-4}\,s^{-1}$ show strength of 93 MPa for the Al and 315 MPa for the steel, respectively.

Figure 11 shows examples of stress–strain curves determined for the Al and for the Al–steel joint material. A complex geometry of the Al–steel joint in the overlap configuration made the evaluation of the shear/tensile strength difficult due to the multi-axial loading system and the complex shear/tensile stress state.[23] However, all tested samples failed in the Al HAZ so the cross-section area of the Al plate was selected to calculate the shear/tensile strength. Interestingly, the shear/tensile strengths of all investigated welds have the same value regardless of the thickness of the brittle intermetallic layers.

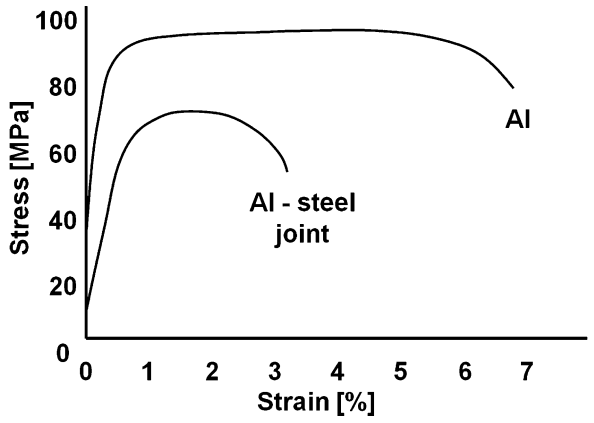

Fig. 11. Stress–strain curves obtained for Al and as-welded sample (laser power: 2.1 kW).

Figure 12 shows a specimen after the shear/tensile test, ruptured in the Al HAZ. Figure 12a and c show the localization of the fracture obtained during shear/tensile test. The fractured surface is shown in detail in Figure 12b where the characteristic appearance for the Al ductile fracture is apparent.

3. Discussion

3.1. Heat Input Measurements and Simulation

Measurements of temperatures during the joining process clearly reveal that the peak temperature at point A as measured by a thermocouple is about 1160 K, which is lower than that at point B obtained by a ratio-pyrometer (Figure 4). In reality, the temperature at the interface (point A) must be higher than that at the Al (point B), because most of the laser power is absorbed by the steel sheet and then the heat is further transferred (through the interface) to the bottom side of the Al sheet. That difference may be caused by the poor contact, i.e., insufficient heat transfer, between the tip of the thermocouple and the measuring point A. Furthermore, the fluid motion caused by the molten Al may also cause a displacement of the thermocouple.

Due to the measured low peak temperature at point A and the difficulty in the precise temperature measurement, the thermal cycle was simulated for each applied laser power. Based on these simulation results, correlations between the thickness of the respective IMP layer and the peak temperature, cooling time, and integral of the thermal cycle can be derived. Figure 13 shows the comparison of the different welding boundary condition parameters (all the values are normalized by the respective maximum occurring values) regarding their respective influence on the resulting intermetallic layer thickness. It is clear that the influence of the peak temperature has the highest relevance.

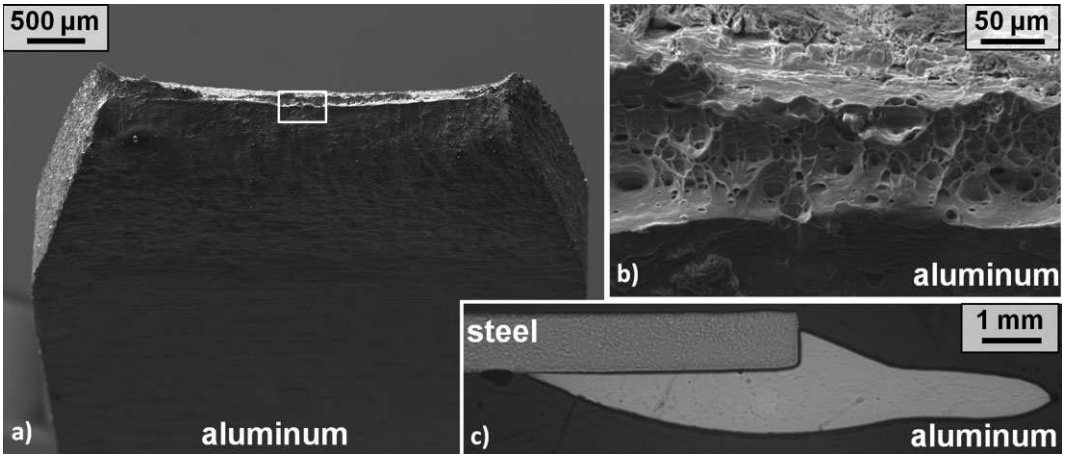

Fig. 12. Macroscopic examination of the fractured surface of the welded sample (laser power 2.1 kW): (a) SEM (SE) overview of the fractured region, (b) SEM (SE) micrograph showing ductile fracture of the Al component, (c) optical microscope (OM) micrograph of the cross-section of the joint.

3.2. Weld Microstructure and Properties

The conductive laser welding process of the dissimilar Al to steel materials in the overlap configuration results in a formation of a complex microstructure of the interface region and therefore its analysis requires a systematic approach: the discussion will follow the thermal history of the interfacial components in a ''scale key'' starting from the largest and finishing with the smallest microstructural features.

Presented in Figure 6 the cross-section of the welded joint provides evidence of the evolution of both parent materials due to the applied thermal cycle. It is obvious that the shape and the size of all zones affected by the laser beam (zones 1–4 in the Al, Figure 6) and (zones A–C in the steel, Figure 6) vary with the applied laser power. The number of specific microstructural regions that can be distinguished in the Al plate changes depending on the heat dissipation through/on the steel plate. It should be mentioned that a distribution of the laser intensity at a work plane is not homogenous. If the work plane is out-of-focus the intensity distribution can become Gaussian.[24] The shape and the size of the zones A–C observed in the steel plate reflect this phenomenon (Figure 6).

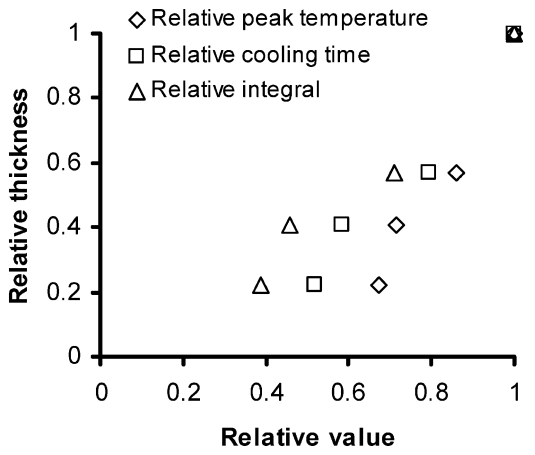

Fig. 13. Correlations between the thicknesses of the respective IMP layers and the peak temperature, cooling time, and integral of thermal cycle from simulations. All values are normalized by the respective maximum occurring values.

The morphology of the final microstructure of the steel (composed mainly of ferrite) depends on the exposure temperature and the cooling rate. However, the higher temperature that the steel plate is exposed to, leads to the bigger grains in the final microstructure (region C in Figure 6). Such a kind of steel microstructure constituent was formed via a displacive transformation,[25] which occurs during shock temperature changes. That explains the local increase of the microhardness (not shown here) of about 80% with respect to the base material.

With decreasing exposure temperature, the size of the grains continuously decreases when moving from zone C to zone B. The followed increment of the grain size in the zone A can be explained by both the primary recrystallization (the generation of new small grains and their further growth at the expanse of the deformed microstructure[26]) and further growth during heating.

While the heat distribution on the top of the steel plate has a Gaussian profile, the heat dissipation and consequently all following microstructural features present at the interface and in the heat affected Al zone are affected by high temperature gradients resulting from the heat flow during the solidification and the cooling of the Al part of the joint. In other words, there is a strong correlation between the applied laser power (the heat accumulated by the steel plate) and the following solidification and the cooling conditions of the Al part. At the fixed welding speed and process set-up (Figure 1 and 2) the amount of heat delivered to the system at unit of time depends only of a laser power. Thus, only laser power determines the steel volume that gains higher temperature than the melting point of the Al.

The heterogeneous heat dissipation then mainly proceeds through the melted and the solidified Al. This process is clearly reflected in the morphology of the Al part of the joint,

ADVANCED ENGINEERING MATERIALS

but also apparent in the fraction and morphology of the IMPs formed at the interface.

The elongation of grains observed in zones 2 and 4 of Figure 6 is caused by a preferential grain growth in the direction of the fastest heat flow. This phenomenon is associated with high temperature gradients that occur in the sample during solidification. The main direction of the heat flow proceeds through the Al plate (Al has the highest thermal conductivity coefficient, k, in this system). The degree of grain elongation in zone 2 increases with decreasing distance to zone 1 which was not melted during the welding process. The thermal conductivity coefficient of the steel is significantly lower than that of the Al but is three orders of the magnitude higher than k of the argon.

The second fastest heat flow direction (through the steel plate) causes the elongation of the grains in zone 4. Consequently the slowest cooling rate within zone 3 is responsible for the formation of equiaxial Al grains.

When the solid Fe interacts with the liquid Al the growth of the intermetallic layer occurs simultaneously with the process of its dissolution in the melt.[27] High heating and cooling rates render the laser beam welding process far from the equilibrium conditions. Those, together with the non-isothermal character of the imposed heating cycle impede the detailed analysis of the role of diffusion,[12] nucleation, and growth processes of the intermetallic reaction layer.

Figure 7 presents in details the constituents of the interface reaction layer, namely, the orthorhombic Al_5Fe_2-phase and the monoclinic $Al_{13}Fe_4$-phase. Our analyses reveal that the interface between the Al_5Fe_2 and the steel tends to flatten with increasing laser power (Figure 8). Eggeler et al.[21] showed similar changes in the interface morphology caused by the increase of the Al melt temperature, while Bouayad in refs.[1,2] proved that perturbations of the steel/Al_5Fe_2 boundary are time-dependent. With respect to the current simulation results (Figure 5a and b) both time and temperature of the reaction between the steel and the Al increase with the applied laser power so that flattening of the interface can be expected. An important mechanism that contributes to the layer-formation kinetics is the dissolution of the Al_5Fe_2-phase in the liquid Al. The rate of formation of the intermetallic compounds equals the differences between its growth rate and the dissolution rate. Studying the relationship between the thickness of the intermetallic layer and the temperature of the Al melt Eremenko et al.[28] proposed a mechanism where at a certain temperature the rate of dissolution exceeds the rate of layer growth. From that point the interlayer thickness decreases with further temperature increase. This limitation of the maximum layer thickness can be a possible explanation of the non-linear growth behavior of the intermetallic reaction layer with the increasing laser power. Another effect of the layer dissolution, reported in ref.,[27] is that unfavorably oriented crystals of Al_5Fe_2 disappear (Figure 7). Consequently, the crystallites of the Al_5Fe_2-phase become more regular and parallel to each other.

According to ref.[2] the $Al_{13}Fe_4$-phase is always present between the Al and the Al_5Fe_2-phase after the interaction between the solid steel and the liquid Al. Changes in the morphology of the $Al_{13}Fe_4$, namely, the formation of plate-like crystallites (Figure 7, 8d, and 10c) was observed in refs.[1,29] In ref.[1] this phenomenon was attributed to the effect of an increasing immersion time of Armco Fe in the Al ($t > 30$ min at 1073 K), while in ref.[29] it was attributed to the effect of an increasing immersion temperature of a structural carbon steel in the Al ($T > 1073$ K for 300 s.). Eggeler et al.[21] proved that needles of the $Al_{13}Fe_4$-phase (Figure 7) are formed during the cooling from the aluminizing temperature. He also compared the microstructure of a sample that was water quenched from the hot-dip aluminizing temperature (987 K) to the microstructure of a sample that was slowly cooled down. Only the microstructure of the second sample reveals needles of the $Al_{13}Fe_4$-phase. Note, that the Al melt that was used in this experiment contained a certain amount of Fe (not specified by the author). According to the current simulation results the cooling rate calculated for joints that were welded with a laser power of 1.7 kW is about 25% higher than in case of the laser power of 2.4 kW ($\approx 240\,K \cdot s^{-1}$). Moreover, an increasing process temperature promotes dissolution of the Fe in the Al melt close to the abutting steel welding partner. An excess of Fe in the Al promotes the precipitation of $Al_{13}Fe_4$ during cooling when the solubility of Fe in the Al decreases.

EBSD investigations of the interface region (Figure 7a) confirmed that the orthorhombic Al_5Fe_2-phase is the dominant component in the reaction layer and the monoclinic $Al_{13}Fe_4$-phase appears at the interface between the Al_5Fe_2-phase and the Al. Moreover, the inverse pole figure map shown in Figure 7b provides evidence of the preferential growth of the Al_5Fe_2-phase. It is a known phenomenon that a high concentration of vacancies along the crystallographic [001] direction facilitates diffusion of Fe atoms (anisotropic diffusion) and hence, promotes the growth of the Al_5Fe_2-phase grains along the c-axis (c-axis corresponds to the [001] direction) of its unit-cell.[30] Its preferential growth direction causes the typical tongue-like morphology of the Al_5Fe_2-phase (Figure 7, 8 and 10).

It needs to be clarified that the width of the intermetallic reaction layer along the interface is not constant but varies according to the distribution of the laser intensity across the spot diameter described above. Our thickness measurements were always performed in the central part of the interface of the joint where the IMP layer was the thickest and also was locally constant.

4. Conclusions

We investigated the correlation between the thermal cycle and the formation of IMPs at the interface of laser-welded Al–steel overlap joints. The following conclusions are drawn:

(1) The applied laser power strongly affects the microstructures of both abutting base materials in the HAZ.

(2) The peak temperature, cooling time, integral of the temperature over time of thermal cycle, and the intermetallic layer thickness are increasing with the laser power.

(3) The influence of the peak temperature on the thickness of the chemical compound layer is two times stronger than the influence of the cooling rate and more than three times stronger than the influence of the integral of the temperature over time.
(4) The morphology of the $Al_{13}Fe_4$-phase is very sensitive with respect to the cooling time.
(5) The thickness of the intermetallic layer was below the critical value that might cause interfacial fracture during shear/tensile loading. Rapture always occurred in the HAZ of the Al alloy and not in the intermetallic layer.

Received: February 21, 2012
Final Version: April 14, 2012
Published online: May 16, 2012

[1] K. Bouche, F. Barbier, A. Coulet, *Mater. Sci. Eng., A* **1998**, *249*, 167.
[2] A. Bouayad, Ch. Gerometta, A. Belkebir, A. Ambari, *Mater. Sci. Eng., A* **2003**, *363*, 53.
[3] L. Agudo, D. Eyidi, C. H. Schmaranzer, E. Arenholz, N. Jank, J. Bruckner, A. R. Pyzalla, *J. Mater. Sci.* **2007**, *42*, 4205.
[4] H. Springer, A. Kostka, J. F. dos Santos, D. Raabe, *Mater. Sci. Eng., A* **2011**, *528*, 4630.
[5] A. Mathieu, R. Shabadi, A. Deschamps, M. Suery, S. Mattei, D. Grevey, E. Cicala, *Opt. Technol.* **2007**, *39*, 652.
[6] R. S. Coelho, A. Kostka, S. Sheikhi, J. F. Dos Santos, A. R. Pyzalla, *Adv. Eng. Mater.* **2008**, *10*, 10.
[7] C. Dharmendra, K. P. Rao, J. Wilden, S. Reich, *Mater. Sci. Eng., A* **2011**, *528*, 1497.
[8] H. Chen, A. J. Pinkerton, L. Li, Z. Liu, A. T. Mistry, *Mater. Des.* **2011**, *32*, 495.
[9] U. R. Kattner, B. P. Burton, in *Alloy Phase Diagrams*, Vol. *3*, ASM International, USA **1992**.
[10] G. V. Kidson, *J. Nucl. Mater. 3* **1961**, *1*, 21.
[11] T. Heumann, S. Dittrich, *Z. Metall.* **1959**, *50*, 617.
[12] P. Peyre, G. Sierra, F. Deschaux-Beaume, D. Stuart, G. Fras, *Mater. Sci. Eng., A* **2007**, *444*, 327.
[13] G. Padmanaban, V. Balasubramanian, *Opt. Laser Technol.* **2010**, *42*, 1253.
[14] E. Schubert, M. Klassen, I. Zerner, C. Walz, G. Sepold, *J. Mater. Process. Technol.* **2001**, *115*, 2.
[15] Z. Sun, J. C. Ion, *J. Mater. Sci.* **1995**, *30*, 4205.
[16] C. Thomy, A. Wirth, M. Kreimeyer, F. Wagner, F. Vollertsen, *Proc. IIW Int. Conference Weld. & Mater, Dubrovnik & Cavtat*, **2007**, 311–326.
[17] I. Zerner, *Prozessstabilisierung und Ergebnisse für das Laserstrahlfügen von Aluminium-Stahl-Verbindungen*, Dissertation University Bremen, BIAS Verlag **2002**.
[18] J. Nocedal, S. Wright, in: *Numerical Optimization*, Springer, Wisconsin **1999**.
[19] C. R. Radscheit, *Laserstrahlfügen von Aluminium mit Stahl*, Dissertation Universität Bremen, BIAS Verlag, **1997**.
[20] V. R. Ryabov, in *Aluminizing of Steel*, Oxonian Press, New Delhi **1985**, 2.
[21] G. Eggeler, W. Auer, H. Kaesche, *Z. Metall.* **1986**, *77*, 239.
[22] H. R. Shahverdi, M. R. Ghomashchi, S. Shabestari, J. Hejazi, *J. Mater. Process. Technol.* **2002**, *124*, 345–352.
[23] G. Sierra, P. Peyre, F. Deschaux Beaume, D. Stuart, G. Fras, *Mater. Charact.* **2008**, *59*, 1705.
[24] D. F. de Lange, J. T. Hofman, J. Meijer, *Influence of intensity distribution on the meltpool and clad shape for laser cladding*, Proceedings of the Third International WLT-Conference on Lasers in Manufacturing, Munich **2005**.
[25] H. K. D. H. Bhadeshia, R. W. K. Honeycombe, *Steel, Microstructure and Properties*, Elsevier, Oxford **2006**, 7–8.
[26] G. Gottstein, *Physical Foundations of Materials Science*, Springer, Berlin **2004**, 304.
[27] V. I. Dybkov, *Reaction Diffusion and Solid State Chemical Kinetics*, The IPSMS Publications, Kyiv **2002**.
[28] V. N. Eremenko, Ya. V. Matanson, V. I. Dybkov, V. R. Ryabov, *Avt. Svarka* **1974**, *2*, 5.
[29] S. Kobayashi, T. Yakou, *Mater. Sci. Eng., A* **2002**, *338*, 44.
[30] V. N. Yeremenko, Ya. V. Natanzon, V. I. Dybkov, *J. Mater. Sci.* **1981**, *16*, 1748.

